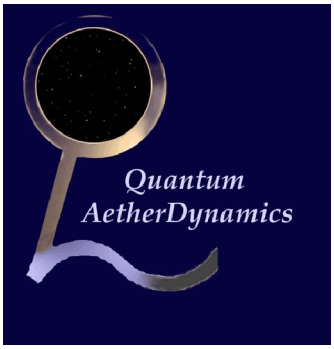

Quantum AetherDynamics Institute (QADI)

Bipolar Trumpet Coils as QMU Toy Models for Black Hole Torsion Filaments and Polar Jets (Analog Torsion)

David W. Thomson III
Quantum AetherDynamics Institute (QADI), Alma, Illinois, USA
ORCID: 0000-0002-5830-5427

Version 1.4 – December 11, 2025

This article is published by the Quantum AetherDynamics Institute (QADI).

It develops the Aether Physics Model (APM)

Abstract

In the Aether Physics Model expressed in Quantum Measurement Units (QMU), black hole environments organize Aether torsion into distinct structures: magnetic torsion filaments associated with the magnetic charge ledger and electrostatic polar jets associated with large-scale potential differences in the electrostatic charge ledger. Because these two charge sectors are reciprocally related in QMU, their torsion manifestations are expected to exhibit a corresponding reciprocity. In particular, a galactic-center black hole is treated as a pure Aether-density configuration whose effective mass ledger is sourced by surrounding galactic matter rather than by interior physical matter, so the torsion structure of its jets is tied directly to the global galactic mass ledger.

This paper develops a unified ledger for these effects and introduces a bipolar double-trumpet Tesla coil as a laboratory toy model of the black hole, accretion ring, and bipolar jet system. The approach is a form of *analog torsion*: the same Aether medium and torsion ledgers govern both the astrophysical system and the coil, so the flow geometry is expected to be scale invariant in QMU. The double-trumpet coil implements two reciprocal torsion phases: a magnetic phase in which ring-like torsion filaments concentrate around the primary winding, and an electrostatic phase in which axial torsion channels form along the conical secondaries and connect to remote top loads.

Using QMU-only invariants built from length density, curl, its reciprocal winding unit, and electrostatic potential, we construct a reciprocal pair of torsion invariants Ξ_{mag} (magnetic filament phase) and Ξ_{elec} (electrostatic jet phase) and interpret Ξ_0 as a total torsion allocation ledger connecting the two. We show that Ξ_{mag}, Ξ_{elec}, and Ξ_0 are determined entirely by already published QMU identities, including the charge-duality relation $\delta_q = 8\pi\alpha$, so the filament–jet reciprocity is a prediction of the existing QMU canon rather than an adjustable parameter.

The black hole event horizon and accretion ring are mapped to the coil waist and primary ring, while the bipolar polar jets are mapped to the two conical secondaries. In this mapping, path shortening along Aether torsion channels appears both in the astrophysical jets and in the laboratory coil as a preference for axial propagation between the coil waist and remote top loads. We propose phase-sensitive QMU experiments in the double-trumpet coil that can test the filament–jet reciprocity, the torsion phase structure, and the path-shortening interpretation of bipolar jets, without attempting to create a literal black hole and without requiring superluminal information transfer.

1 Introduction

In the Aether Physics Model (APM), the physical vacuum is modeled as a quantized Aether composed of discrete space quanta, with charge distributed over toroidal geometries and dynamics expressed in Quantum Measurement Units (QMU) [Thomson and Bourassa, 2004]. The propagation of photons, the organization of charge, and the phenomena attributed to gravity all arise from the geometry and torsion of this Aether, with mass–energy ledgers providing the bridge between Aether geometry and relativistic observables [Thomson, 2025b]. The QMU decomposition of the propagation constant,

$$A_u \,\mathrm{curl} \;=\; {F_q}^2 {\lambda_C}^2, \tag{1}$$

defines the Aether unit A_u and the torsion unit curl as the rotational and torsional factors of the propagation constant, with $F_q\lambda_C$ as the photon speed. This identity (Ledger One) is the starting point for all torsion analysis and has been used to construct mass–energy and chronovibrational ledgers in several QMU applications [Thomson, 2025b,c].

In the APM, a galactic-center black hole is not a lump of interior matter surrounded by an accretion flow, but a self-consistent Aether-density configuration whose effective mass ledger is supplied by

the surrounding galactic matter [Thomson III, 2025]. The "mass of the black hole" is therefore a shorthand for a central Aether-density gradient anchored by the galaxy as a whole, rather than for physical matter located inside the event horizon. Collapsing objects such as neutron stars can transiently seed such configurations, but once the Aether-density structure is established, the physical matter evaporates and the ledger is carried entirely by the Aether.

Around these rotating Aether-density configurations, the Aether torsion organizes into structures. Previous QMU work identified magnetic torsion filaments—thin, magnetically dominated strands—near galactic centers and on cosmic-web scales [Thomson, 2025d,a], in qualitative agreement with the nonthermal radio filament systems observed in the Galactic Center [Yusef-Zadeh et al., 1984, Morris and Serabyn, 1996, Yusef-Zadeh, 2003]. These are associated with the magnetic charge ledger, including the maximum magnetic charge ${e_{\mathrm{emax}}}^2$ and the Aether magnetic charge ${e_a}^2$. At the same time, many black holes exhibit bipolar polar jets with large-scale potential differences along their axes, as in active galactic nuclei (AGN), blazars, and X-ray binaries [Blandford and Znajek, 1977, Blandford and Payne, 1982, Blandford et al., 2019, Urry and Padovani, 1995, Mirabel and Rodríguez, 1999, Remillard and McClintock, 2006, Event Horizon Telescope Collaboration, 2019]. In the APM, these jets are naturally interpreted as electrostatic torsion channels driven by the electrostatic charge ledger e^2 and its potential differences.

Because the electrostatic and magnetic charge units are reciprocally related,

$$\delta_q \equiv \frac{e^2}{{e_{\mathrm{emax}}}^2}, \tag{2}$$

one expects their torsion manifestations to exhibit a corresponding reciprocity. Magnetic torsion filaments and electrostatic polar jets should be dual phases of the same underlying Aether torsion geometry, with their mathematical descriptions related by a charge-duality transformation. In one phase, the torsion is organized into azimuthal filaments around the compact object; in the dual phase, the torsion is organized into axial channels along the polar directions.

The goal of this paper is to formalize this reciprocity in QMU and to propose a laboratory toy model that implements the same torsion physics in a controllable setting. The toy model is a bipolar double-trumpet Tesla coil: two conical secondaries joined at their open horns, with a single primary wrapped around the joined ring. This geometry closely matches the black hole plus accretion ring plus bipolar jet configuration. The present work is thus a case of *analog torsion*: the same Aether and the same QMU torsion ledgers are applied to both astrophysical and laboratory systems, so the underlying geometry of the flow is expected to be scale invariant in QMU even though the physical scales differ dramatically. This is analogous in spirit to analogue-gravity experiments that simulate horizons and Hawking radiation in condensed-matter systems, but applied here to the torsion sector of the Aether instead of curvature in an effective metric [Barceló et al., 2011, Steinhauer, 2016, Jacquet et al., 2020].

We show that the double-trumpet coil can be used to test the Aether torsion phase structure, the filament–jet reciprocity, and the path-shortening effect in a finite, non-singular system. The experimental emphasis is on phase and chronovibrational shifts, not on superluminal signaling. The coil is used to verify the general QMU torsion laws that apply to black holes and their jets, not to emulate massive gravitational singularities or concentrate physical matter inside an event horizon.

2 QMU preliminaries: length density, curl, and winding

2.1 Length density as a mass–radius ledger

A central concept in the present analysis is the *length density*, defined as the ratio of mass to radius. For a spherically symmetric mass distribution $M(r)$, the length density is

$$\Lambda(r) \equiv \frac{M(r)}{r}. \tag{3}$$

In QMU, it is convenient to work with a dimensionless ledger

$$\Lambda^*(r) \equiv \frac{M(r)/m_a}{r/\lambda_C} = \frac{M(r)}{m_a}\,\frac{\lambda_C}{r}, \tag{4}$$

which measures the mass per radial quantum in units of the Aether mass unit m_a and the Compton length λ_C. Large Λ^* indicates many Aether mass quanta per radial interval; small Λ^* indicates a sparse mass ledger. Length-density ledgers have already been applied to galactic-center torsion filaments and cosmic-web structures within QMU [Thomson, 2025d,a].

For a galactic-center black hole in the Aether Physics Model, $M(r)$ is not the sum of "black-hole mass plus external galactic mass" in the usual sense. Instead, $M(r)$ is the *effective mass ledger* of the surrounding galactic matter that has been pulled into the central Aether density gradient. There is no additional reservoir of physical matter inside the event horizon; the black hole is a self-consistent Aether-density configuration whose ledger is sourced by the galaxy as a whole [Thomson III, 2025]. The Aether Lagrangian for the galaxy–black-hole system therefore links the event-horizon radius directly to the global galactic mass ledger, so that

$$\rho_{\rm EH} \equiv \frac{R_{\rm EH}}{\lambda_C} = f\!\left(\frac{M_{\rm gal}}{m_a}\right), \tag{5}$$

where $M_{\rm gal}$ is the mass ledger of the host galaxy in QMU. Neutron-star–initiated black holes appear as a special, transient case in which collapsed matter briefly seeds the Aether-density configuration before the physical matter evaporates and the ledger is carried entirely by the Aether geometry.

A particularly important reference point is the extremal galactic-center condition in which the Aether mass ledger and length ledger satisfy

$$\frac{M}{r} = \frac{m_a}{\lambda_C}, \qquad \text{curl} = 1. \tag{6}$$

At this point the dimensionless length-density ledger is $\Lambda^* = 1$, but the associated Aether fine structure $\alpha_{\rm A}$ for the galactic-center configuration is extremely small, of order 10^{-48} in QMU, because the mass ledger has been driven to the maximum Aether mass scale m_a while the curl unit remains fixed. This scale separation is central to the distinction between true galactic-center black holes and laboratory analogues: the torsion unit curl is scale invariant, but the combination of length density and fine structure determines whether the system occupies the galactic-center ledger point or an electron-scale regime.

2.2 Curl and its reciprocal winding unit

The QMU torsion unit is defined by

$$\text{curl} = \frac{{e_{\rm emax}}^2}{m_{\rm e}\lambda_C}, \tag{7}$$

which ties the torsion directly to the magnetic charge ${e_{\rm emax}}^2$ and the electron mass $m_{\rm e}$ [Thomson and Bourassa, 2004, Thomson, 2025b]. Physically, curl measures the torsional twist per Aether quantum.

The reciprocal of curl defines a *winding unit*,

$$\text{perm} \equiv \frac{1}{\text{curl}} = \frac{m_{\rm e}\lambda_C}{{e_{\rm emax}}^2}. \tag{8}$$

In coil analogies, perm represents the effective number of windings encoded in the torsion geometry. Large curl corresponds to strong torsion per Aether quantum; large perm corresponds to many effective windings distributed along a path. The trumpet coil geometry is specialized for redistributing the same underlying torsion budget between these two expressions.

2.3 Charge-duality and electrostatic curl analogue

The electrostatic and magnetic charge units are related by

$$\delta_q \equiv \frac{e^2}{{e_{\rm emax}}^2}, \tag{9}$$

and QMU analysis of trumpet-coil systems and superconducting ledgers identifies this ratio with the fine-structure constant via

$$\delta_q = 8\pi\alpha, \tag{10}$$

within the empirical precision of those experiments [Thomson and Bourassa, 2004, Thomson, 2025c]. From this, an electrostatic analogue of the torsion unit follows:

$$\text{curl}_{\rm elec} \equiv \frac{e^2}{m_{\rm e}\lambda_C} = \delta_q\,\text{curl} = 8\pi\alpha\,\text{curl}. \tag{11}$$

The pair $(\text{curl}, \text{curl}_{\rm elec})$ provides two dual handles on the Aether torsion geometry: one weighted by the magnetic charge ledger and one weighted by the electrostatic charge ledger. Magnetic torsion filaments are associated with curl and ${e_{\rm emax}}^2$; electrostatic polar jets are associated with $\text{curl}_{\rm elec}$ and e^2 along with large-scale potential differences.

3 Black hole torsion phases in QMU

3.1 Magnetic torsion filaments

Around rotating black holes, the Aether torsion can organize into magnetic torsion filaments: narrow, magnetically dominated strands aligned with the local torsion field. These arise when a torsion invariant constructed from the length density and its gradient exceeds a threshold. Using the QMU mass–energy ledger, the Aether unit, and the charge-duality identity $\delta_q = 8\pi\alpha$, the filament threshold can be written in fully dimensionless form as

$$\boxed{\Xi_{\rm mag} = 8\pi\alpha\,\Lambda^*_{\rm toroid}\left|\frac{\partial\Lambda^*_{\rm toroid}}{\partial(r/\lambda_C)}\right|} \quad \text{(magnetic filament invariant)}, \tag{12}$$

where $\Lambda^*_{\rm toroid}$ is the toroidal length-density ledger in the near-horizon region [Thomson, 2025d,a]. Critical filamentation occurs when

$$\Xi_{\rm mag} \gtrsim 1. \tag{13}$$

These filaments are the QMU representation of observed nonthermal radio filaments near galactic centers and on cosmic scales [Yusef-Zadeh et al., 1984, Morris and Serabyn, 1996, Yusef-Zadeh, 2003, Thomson, 2025a]. Their clustering and spacing reflect the underlying length-density and torsion ledgers of the host system.

3.2 Electrostatic polar jets

In many black hole systems, torsion manifests instead, or in addition, as bipolar polar jets: narrow axial channels with large-scale potential differences along them [Blandford and Znajek, 1977, Blandford and Payne, 1982, Blandford et al., 2019, Urry and Padovani, 1995, Mirabel and Rodríguez, 1999, Remillard and McClintock, 2006]. In QMU, these jets are associated with the electrostatic charge ledger e^2 and a potential difference $\Delta\Phi(z)$ between regions along the polar axis. The axial Aether geometry is characterized by an electrostatic torsion invariant

$$\boxed{\Xi_{\rm elec} = \frac{1}{8\pi\alpha}\,\Lambda^*_{\rm axis}\left|\frac{\partial\Lambda^*_{\rm axis}}{\partial(z/\lambda_C)}\right|\left(\frac{\Delta\Phi}{\Phi_0}\right)} \qquad \text{(electrostatic jet invariant)}, \tag{14}$$

where $\Lambda^*_{\rm axis}$ is the axial length-density ledger and

$$\Phi_0 \equiv \frac{e^2}{4\pi\epsilon_0\,\lambda_C} \tag{15}$$

is the natural QMU electrostatic potential quantum, the potential of an elementary distributed electrostatic charge at one Compton wavelength in standard notation. In both astrophysical jets and trumpet-coil geometries, the axial potential difference that actually appears tends to be of order $\Delta\Phi \sim \Phi_0$, so the factor $\Delta\Phi/\Phi_0$ is an order-one multiplier in the threshold analysis. Electrostatic jet formation corresponds to

$$\Xi_{\rm elec} \gtrsim 1. \tag{16}$$

3.3 Reciprocity and torsion allocation

Because curl and perm are reciprocal, and e^2 and ${e_{\rm emax}}^2$ are reciprocally related via $\delta_q = 8\pi\alpha$, the product of the two invariants is approximately constant in the ideal symmetric case where the toroidal and axial gradient geometries match:

$$\boxed{\Xi_0 \equiv \Xi_{\rm mag}\,\Xi_{\rm elec} = \left(\frac{\Delta\Phi}{\Phi_0}\right)\times\mathcal{O}(1) \approx 1,} \tag{17}$$

where the $\mathcal{O}(1)$ factor encodes small geometric differences between toroidal and axial configurations. In the idealized $\Delta\Phi \simeq \Phi_0$ case, $\Xi_0 \simeq 1$ exactly. Thus the *total torsion allocation* ledger Ξ_0 is a derived quantity, not a free parameter.

It is often convenient to write the reciprocity directly as

$$\Xi_{\rm elec} = \frac{\Xi_0}{\Xi_{\rm mag}}, \tag{18}$$

with $\Xi_0 \simeq 1$ set by the underlying QMU constants. This relation can be interpreted as an approximate conservation of a total torsion budget: the Aether torsion around the compact object is apportioned between the filament phase and the jet phase.

Three torsion phases are then distinguished:

- **Magnetic filament phase:** $\Xi_{\rm mag} \gg 1$ and $\Xi_{\rm elec} \ll 1$. The torsion geometry favors a network of magnetic filaments, with suppressed polar jets.
- **Electrostatic jet phase:** $\Xi_{\rm elec} \gg 1$ and $\Xi_{\rm mag} \ll 1$. The torsion geometry favors bipolar polar channels, with a simplified or reorganized filament network.
- **Mixed phase:** $\Xi_{\rm mag} \sim 1$ and $\Xi_{\rm elec} \sim 1$. Both filamentary and axial structures coexist, resembling the transition region of a trumpet coil between its wide horn and narrow point.

In this phase picture it is important to distinguish between the *dimensionless* thresholds $\Xi_{\rm mag} \sim 1$, $\Xi_{\rm elec} \sim 1$ and the *absolute* ledger scale of the system. A galactic-center black hole occupies the extremal length-density point $M/r = m_a/\lambda_C$ with curl $= 1$ and an extremely small Aether fine structure $\alpha_{\rm A} \sim 10^{-48}$, whereas an electron-sector system such as a Tesla coil operates with the same torsion unit curl but with the electron mass ledger and fine structure α. The invariants $\Xi_{\rm mag}$ and $\Xi_{\rm elec}$ can reach order unity in both regimes, but the underlying ledgers differ by many orders of magnitude. The toy models considered later in this paper probe the *phase structure* of torsion—how a fixed torsion unit is partitioned between filaments and jets—without ever approaching the galactic-center extremal length density or Aether fine structure.

Filament–jet reciprocity ledger (explicit form). The Aether torsion geometry around rotating compact objects is controlled by two dimensionless invariants:

$$\Xi_{\rm mag} = 8\pi\alpha\, \Lambda^*_{\rm toroid} \left| \frac{\partial \Lambda^*_{\rm toroid}}{\partial (r/\lambda_C)} \right|, \tag{19}$$

$$\Xi_{\rm elec} = \frac{1}{8\pi\alpha}\, \Lambda^*_{\rm axis} \left| \frac{\partial \Lambda^*_{\rm axis}}{\partial (z/\lambda_C)} \right| \left(\frac{\Delta\Phi}{\Phi_0} \right), \tag{20}$$

$$\Xi_0 \equiv \Xi_{\rm mag}\, \Xi_{\rm elec} \;\approx\; 1. \tag{21}$$

The constant Ξ_0 is a derived total torsion allocation ledger, fixed by the QMU charge-duality identity $\delta_q = 8\pi\alpha$ up to order-one geometric factors. The magnetic filament phase, electrostatic jet phase, and mixed phase are determined by whether $\Xi_{\rm mag}$ or $\Xi_{\rm elec}$ exceeds unity, while the absolute ledger scale (galactic-center versus electron sector) is set by the combination of length density and fine structure.

4 Bipolar double-trumpet coils as toy models

4.1 Geometry of the double-trumpet coil

The bipolar double-trumpet coil consists of two conical secondary coils joined at their wide ends (the "horns"), with a single primary winding wrapped around the ring where the horns meet. Each secondary extends from the horn ring to a narrow point along an axis, and may be terminated in a top load located at some distance from the coil. The geometry is symmetric with respect to the horn ring.

A direct mapping to the black hole system is:

- **Horn ring and primary:** analog of the black hole horizon and inner accretion ring, where the length density and torsion are highest in a toroidal region.
- **Double cones (secondaries):** analogs of the two polar torsion channels, one in each direction along the axis.
- **Remote top loads:** analogs of the remote anchor regions joined by the polar jets, where energy and matter accumulate in the astrophysical case.

The primary current concentrates near the horn ring, creating a toroidal Aether torsion pattern analogous to the environment just outside the horizon. The conical secondaries redistribute the torsion and potential, functioning as trumpet-like torsion channels. Trumpet and non-uniform-pitch coil geometries are known experimentally to redistribute current and potential along the winding [Tesla, 1893, Melo and Neves, 2021, Reed et al., 2015], providing a practical platform for analog torsion tests.

4.2 Length density and the mass–energy ledger in the coil

In the coil, the length density ledger is not literal rest mass per radius, but an effective mass ledger associated with the stored Aether field energy. In the APM, the mass–energy ledger equates field energy to an effective Aether mass, so that a field configuration with energy E contributes an amount E/m_a to the mass ledger in QMU units [Thomson and Bourassa, 2004, Thomson, 2025b].

For a toroidal shell around the primary, we define an effective length density

$$\Lambda^*_{\rm ring} \equiv \frac{E_{\rm ring}/m_a}{r_{\rm ring}/\lambda_C}, \tag{22}$$

where $E_{\rm ring}$ is the field energy in the ring region and $r_{\rm ring}$ is the horn radius. Along the axis of a secondary, we define similarly

$$\Lambda^*_{\rm axis}(z) \equiv \frac{E_{\rm axis}(z)/m_a}{z/\lambda_C}, \tag{23}$$

with z measured from the horn ring along the cone axis. In both cases, the use of E/m_a reflects the QMU mass–energy ledger that treats field energy as an Aether mass contribution.

The torsion and winding units curl and perm are properties of the Aether, not of the specific coil. The coil geometry and winding count determine how much of the torsion budget is expressed as local magnetic twist around the ring (magnetic phase) versus axial winding along the cones (electrostatic phase). However, the *ledger scale* of the trumpet coil is fixed by the electron mass and the fine structure α: even when $\Xi^{\rm coil}_{\rm mag}$ and $\Xi^{\rm coil}_{\rm elec}$ reach order unity, the effective length density and Aether fine structure remain many orders of magnitude away from the galactic-center condition $M/r = m_a/\lambda_C$ with $\alpha_{\rm A} \sim 10^{-48}$. The coil can therefore reproduce the torsion *phase structure* and reciprocity, but it can never realize a galactic-center black hole.

4.3 Trumpet behavior: current and potential

In a single trumpet coil, experiments show that the current is highest in the wide horn region while the electrostatic potential is highest at the narrow point, as expected for non-uniform-pitch helical resonators [Melo and Neves, 2021, Tesla, 1893]. This matches the QMU phase picture:

- In the horn region, the Aether torsion is expressed primarily in azimuthal directions: high effective curl, modest potential differences. This is the analog of the magnetic filament phase near a black hole.
- Near the point, the Aether torsion is expressed as axial winding: high effective perm and large potential differences along the axis. This is the analog of the electrostatic jet phase.

The double-trumpet coil generalizes this to a bipolar configuration, with a single primary ring feeding two trumpet phases in opposite directions along the axis.

5 Filament and jet invariants in the coil

5.1 Magnetic torsion filaments around the primary

Around the primary ring, the coil is expected to exhibit analogs of magnetic torsion filaments when the effective magnetic invariant

$$\Xi_{\mathrm{mag}}^{\mathrm{coil}} \;=\; 8\pi\alpha\,\Lambda_{\mathrm{ring}}^{*}\left|\frac{\partial\Lambda_{\mathrm{ring}}^{*}}{\partial(r/\lambda_C)}\right| \tag{24}$$

exceeds a coil-specific threshold. This can manifest experimentally as discrete azimuthal hot spots or bands where the local field intensity and energy density are enhanced relative to the average, observable with fluorescent probes or field-mapping techniques.

The mapping between the astrophysical and coil invariants is

$$\Xi_{\mathrm{mag}}^{\mathrm{coil}} \;\longleftrightarrow\; \Xi_{\mathrm{mag}}^{\mathrm{BH}}, \tag{25}$$

with $\Lambda_{\mathrm{ring}}^{*}$ playing the role of the near-horizon length-density ledger and the primary current setting the effective torsion strength. This is the analog-torsion realization of the toroidal filament environment inferred near galactic centers [Thomson, 2025d, Morris and Serabyn, 1996].

5.2 Electrostatic torsion channels along the cones

Along each cone axis, when the top loads are placed at a suitable distance and the coil is driven at a resonant condition, the axial invariant

$$\Xi_{\mathrm{elec}}^{\mathrm{coil}} \;=\; \frac{1}{8\pi\alpha}\,\Lambda_{\mathrm{axis}}^{*}(z)\left|\frac{\partial\Lambda_{\mathrm{axis}}^{*}}{\partial(z/\lambda_C)}\right|\left(\frac{\Delta\Phi_{\mathrm{axis}}}{\Phi_0}\right) \tag{26}$$

can exceed its threshold. Here $\Delta\Phi_{\mathrm{axis}}$ is the potential difference between the horn region and the remote top load, expressed in QMU via e^2. In this regime, the coil supports electrostatic torsion channels: preferred Aether paths between the horn ring and the remote loads, analogs of astrophysical polar jets.

The mapping is

$$\Xi_{\mathrm{elec}}^{\mathrm{coil}} \;\longleftrightarrow\; \Xi_{\mathrm{elec}}^{\mathrm{BH}}, \tag{27}$$

with $\Lambda_{\mathrm{axis}}^{*}$ matching the axial length-density profile in the black hole jet and $\Delta\Phi_{\mathrm{axis}}$ matching the large-scale potential difference along the polar axis [Blandford et al., 2019, Event Horizon Telescope Collaboration, 2019].

5.3 Reciprocal phase structure

In the double-trumpet coil, the filament and jet invariants are expected to satisfy a reciprocal relation analogous to (18),

$$\Xi_{\mathrm{elec}}^{\mathrm{coil}} = \frac{\Xi_0^{\mathrm{coil}}}{\Xi_{\mathrm{mag}}^{\mathrm{coil}}}, \tag{28}$$

where Ξ_0^{coil} is a coil-specific realization of the total torsion allocation ledger, differing from unity only by geometric factors and by modest deviations of $\Delta\Phi_{\mathrm{axis}}$ from Φ_0. By varying the primary drive amplitude, frequency, and top-load distance, one can move the coil through the three torsion phases:

- **Filament-dominated regime:** large ring energy density, modest axial potential difference. $\Xi_{\mathrm{mag}}^{\mathrm{coil}}$ is large, $\Xi_{\mathrm{elec}}^{\mathrm{coil}}$ is small. The coil exhibits strong ring filaments and weak axial channels.
- **Jet-dominated regime:** tuned axial resonance and large axial potential difference. $\Xi_{\mathrm{elec}}^{\mathrm{coil}}$ is large, $\Xi_{\mathrm{mag}}^{\mathrm{coil}}$ is small. The coil exhibits strong axial channels and a simplified ring filament pattern.
- **Mixed regime:** intermediate drive and geometry. Both ring filaments and axial channels are present, analogous to environments where both torsion filaments and polar jets are observed in AGN and X-ray binaries [Fender et al., 2004, Blandford et al., 2019].

6 Path shortening in jets and in the coil

6.1 Path-shortened null trajectories

In torsion-dominated regions, null trajectories in the Aether do not follow straight lines in the Euclidean sense. Instead, they follow loxodromic or helical geodesics that can *shorten the coordinate distance* between events while preserving the local photon speed $F_q\lambda_C$. If $d\ell_0$ is the coordinate length element in a weak-torsion region and $d\ell_{\mathrm{tors}}$ is the corresponding element in a torsion channel, then

$$d\ell_{\mathrm{tors}} = \chi(\Xi)\, d\ell_0, \qquad 0 < \chi(\Xi) \leq 1, \tag{29}$$

where Ξ is the relevant torsion invariant (magnetic or electrostatic) and $\chi(\Xi)$ is a dimensionless path-shortening factor. The local relation between coordinate length and time remains

$$d\ell_{\mathrm{tors}} = F_q\lambda_C\, dt. \tag{30}$$

All path-shortening effects arise from $\chi(\Xi)$, not from any change in $F_q\lambda_C$. In the QMU mass–energy ledgers, such path shortening has already been considered for chronovibrational and relativistic potential effects [Thomson, 2025b, Thomson III, 2025].

6.2 Black hole jets as path-shortened channels

In the electrostatic jet phase around black holes, the axial invariant $\Xi_{\mathrm{elec}}^{\mathrm{BH}}$ determines the Aether geometry along the polar axis. The corresponding path-shortening factor $\chi_{\mathrm{jet}}(\Xi_{\mathrm{elec}}^{\mathrm{BH}})$ controls how much shorter the null paths are between the near-horizon region and the remote anchor regions joined by the jets, relative to a weak-torsion Aether. This provides a natural QMU interpretation of

apparently superluminal motions in AGN and microquasar jets [Rees, 1966, Mirabel and Rodríguez, 1999]: the local photon speed ledger remains intact, while the coordinate distance along the torsion channel is effectively shortened.

The jets can thus be viewed as *path-shortened Aether channels* rather than merely ballistic outflows. The black hole latches onto distant regions of space via these torsion channels, and these regions participate in the same Aether ledger as the central Aether-density configuration.

6.3 Path-shortening and phase in the double-trumpet coil

In the double-trumpet coil, the jet analogue is the axial torsion channel between the horn ring and the remote top loads. When $\Xi_{\text{elec}}^{\text{coil}}$ is large, a path-shortening factor $\chi_{\text{coil}}(\Xi_{\text{elec}}^{\text{coil}})$ can be defined such that null or near-null signals in the Aether prefer the axial channel over off-axis paths of the same Euclidean distance.

In practice, the most accessible observable is not a time-of-flight difference for information-bearing pulses, but a *phase or chronovibrational shift* for a modulated signal. A modulated excitation applied at the horn region can be detected:

- Along the axis between horn and top load (torsion channel);
- At the same geometric radius but displaced off-axis (reference path).

A difference in phase accumulation between these paths is interpreted as a difference in effective coordinate path length in the Aether geometry, not as a change in the local photon speed. The experiment is designed to measure how the torsion geometry alters phase, not to demonstrate superluminal information transfer.

> **Path-shortening and phase ledger.** For both black hole jets and the double-trumpet coil, the Aether torsion controls a path-shortening factor $\chi(\Xi)$ that modifies coordinate path lengths while preserving the photon speed:
>
> $$d\ell_{\text{tors}} = \chi(\Xi)\, d\ell_0, \tag{31}$$
> $$d\ell_{\text{tors}} = F_q \lambda_C\, dt. \tag{32}$$
>
> In laboratory tests, the observable is a phase or chronovibrational shift between torsion-channel paths and reference paths, not an information speed greater than $F_q \lambda_C$.

7 Experimental program in QMU

7.1 Phase mapping in the filament regime

The first class of experiments uses the double-trumpet coil to map the filament-dominated regime:

1. Configure the top loads so that the axial potential difference is modest (short separation or no top loads).
2. Drive the coil near its primary resonance, with moderate input power such that $\Lambda_{\text{ring}}^{*}$ is substantial but $\Lambda_{\text{axis}}^{*}$ remains small.

3. Use small fluorescent tubes, neon indicators, or field probes placed around the horn ring to detect azimuthal variations in field intensity and phase.

The expectation is that the ring will exhibit discrete hot spots or filamentary structures where $\Xi_{\mathrm{mag}}^{\mathrm{coil}}$ is locally enhanced, analogous to astrophysical torsion filaments around the accretion ring [Thomson, 2025d, Morris and Serabyn, 1996].

7.2 Phase mapping in the jet regime

The second class of experiments explores the jet-dominated regime:

1. Move the top loads to distances that produce a large potential difference along the cone axes.
2. Adjust the drive frequency to match the axial resonance of the secondary and top-load combination.
3. Monitor both the ring region and the remote loads for discharge activity, field intensity, and phase response to a modulated drive.

In this regime, field concentration and discharge should shift towards the remote loads. The coil should display axial channels of enhanced activity, while the ring filament pattern simplifies. To probe path-shortening, a phase-locked modulation can be applied at the horn and measured both at the top loads and at off-axis reference points. A systematic phase difference consistent with a shorter effective path along the axial channel supports the path-shortening interpretation.

7.3 Mixed and transition regimes

By continuously varying the top-load distance and drive conditions, the coil can be moved through mixed regimes where both ring filaments and axial channels coexist. Mapping the response of the coil in this two-parameter space $(\Lambda_{\mathrm{ring}}^{*}, \Delta\Phi_{\mathrm{axis}})$ provides a laboratory phase diagram for Aether torsion, with $(\Xi_{\mathrm{mag}}^{\mathrm{coil}}, \Xi_{\mathrm{elec}}^{\mathrm{coil}})$ as the controlling variables. This phase diagram is the analog-torsion representation of the state structure seen in active galactic nuclei and related systems [Fender et al., 2004, Blandford et al., 2019].

7.4 Caution on information speed

It is important to distinguish between different velocities in the coil system. Phase velocity and various pattern velocities can exceed $F_q\lambda_C$ without carrying information faster than $F_q\lambda_C$. The QMU torsion analysis here is restricted to geometric path shortening and phase effects. The experimental program is not to demonstrate superluminal information transfer, but to show that the Aether torsion geometry in the coil behaves as the analog-torsion counterpart of the black hole jet geometry. All information-bearing signals are assumed to respect the local photon speed $F_q\lambda_C$.

7.5 Methodology for detecting Aether path shortening

To distinguish genuine QMU path shortening from standard waveguide phase velocities or inductive coupling delays, we propose a differential latency experiment using the double-trumpet coil. The core

observable is not the absolute velocity, but the *power-dependent variation* in the signal time-of-flight or phase, which correlates with the torsion invariant Ξ_{elec} via the path-shortening factor $\chi(\Xi)$.

Experimental setup

The apparatus consists of the bipolar double-trumpet coil configured with remote top loads at a fixed geometric distance z_{load} from the horn ring. The system is driven by a modulated RF source at the coil's resonant frequency f_0.

- **Signal source:** A carrier wave at f_0, amplitude-modulated by a sharp pulse or square-wave train with modulation frequency $f_{\text{mod}} \ll f_0$. The modulation envelope represents the chronovibrational signal whose latency and phase are measured.
- **Probes:** Two identical broadband E-field probes. Probe A is located at the horn ring (source, time stamp t_0). Probe B is located at the top load (destination, time stamp t_1).
- **Data acquisition:** A high-bandwidth, optically isolated oscilloscope or equivalent chronovibrational recorder compares the arrival time and phase of the modulation envelope between Probe A and Probe B.

The coordinate distance

$$\Delta\ell_0 \;=\; z_{\text{load}}$$

is fixed rigidly in Euclidean space. All observed changes in latency are therefore attributed either to conventional circuit effects or to changes in the Aether path-shortening factor $\chi(\Xi)$.

Protocol

The experiment proceeds by varying the input power P_{in}, which directly modulates the length-density ledgers Λ^*_{ring} and Λ^*_{axis} and the torsion invariant Ξ_{elec}, without changing the geometry.

1. **Null baseline (low Ξ):** The coil is driven at the minimum power required to detect the modulation envelope at Probe B. In this limit, $\Xi_{\text{elec}} \to 0$ and $\chi(\Xi) \to 1$. The baseline time-of-flight or envelope latency $\Delta t_{\text{base}} = t_1 - t_0$ is recorded, together with the baseline phase difference.
2. **Thermal control:** To decouple thermal effects (resistance changes in the copper windings) from torsion effects, the coil is either operated in short, low-duty-cycle bursts to maintain a nearly constant average temperature, or allowed to reach thermal equilibrium at each power step before measurement. The DC resistance of the primary is monitored as a proxy for temperature, and any RLC parameter drift is recorded.
3. **Torsion ramp (increasing Ξ):** The input power P_{in} is stepped up in increments. At each step, Ξ_{elec} increases through the mass–energy and torsion ledgers, and the QMU prediction is that the effective path length shortens to

   $$\Delta\ell_{\text{tors}} \;=\; \chi(\Xi)\,\Delta\ell_0, \qquad \chi(\Xi) < 1,$$

   once the jet-like torsion channel is established.
4. **Measurement:** At each power level, the observed latency $\Delta t_{\text{obs}}(P)$ and phase difference are recorded, and the deviation

   $$\delta t(P) \;=\; \Delta t_{\text{obs}}(P) - \Delta t_{\text{base}}$$

is computed. In parallel, off-axis reference probes at the same geometric radius monitor any global drift or thermal effects in the electronics.

Predicted signature

Standard electrodynamics, with linear and time-invariant components, predicts that the group velocity of the modulation envelope is determined by the fixed inductance, capacitance, and resistance of the structure. While this velocity may differ from $F_q\lambda_C$ in conventional units, it should remain effectively constant as long as the coil and environment do not change except for well-characterized thermal effects. Any residual phase shifts due purely to RLC drift can be tracked via resistance monitoring and off-axis reference probes [Reed et al., 2015, Melo and Neves, 2021].

In contrast, the Aether Physics Model predicts a *power-dependent decrease* in effective latency along the torsion channel that cannot be explained by ordinary RLC parameter changes alone. As P_{in} increases, the Aether organizes into a tighter axial torsion channel (larger Ξ_{elec} and smaller $\chi(\Xi)$), effectively bringing the top load "closer" in Aether coordinates. In QMU terms, this appears as a negative derivative

$$\frac{d\,\Delta t_{\mathrm{obs}}}{dP_{\mathrm{in}}} \;<\; 0, \tag{33}$$

after correcting for thermal drift, nonlinear component behavior, and any changes in the off-axis reference paths.

A statistically significant, repeatable trend with $d\Delta t_{\mathrm{obs}}/dP_{\mathrm{in}} < 0$, correlated with the onset of the jet-dominated torsion phase and not reproducible by ordinary RLC parameter changes, would constitute evidence for the path-shortening ledger $\chi(\Xi)$ in the coil. The interpretation remains geometric: the modulation envelope follows a shorter effective Aether path, while the local photon-speed ledger $d\ell_{\mathrm{tors}} = F_q\lambda_C\,dt$ is preserved.

8 Discussion and outlook

In this paper, black hole torsion filaments and polar jets have been treated as reciprocal manifestations of Aether torsion in the Aether Physics Model, controlled by a pair of dimensionless torsion invariants Ξ_{mag} and Ξ_{elec} built from length density, torsion, winding, and potential differences in QMU. The explicit forms (12)–(17) show that these invariants are not phenomenological constructs but follow directly from already published QMU identities, including the charge-duality relation $\delta_q = 8\pi\alpha$ [Thomson and Bourassa, 2004, Thomson, 2025c,d,a]. The reciprocal relation between Ξ_{mag} and Ξ_{elec} reflects the reciprocal relationship between the electrostatic and magnetic charge units and suggests an approximate conservation of a total torsion allocation ledger. Because the total torsion allocation constant Ξ_0 is fixed by the previously published QMU charge-duality identity $\delta_q = 8\pi\alpha$ (up to order-one geometric factors and the ratio $\Delta\Phi/\Phi_0$), the filament–jet reciprocity is a prediction of the existing QMU canon rather than a new adjustable parameter.

A second key point is the treatment of galactic-center black holes as pure Aether-density configurations whose effective mass ledger is sourced entirely by the surrounding galactic matter [Thomson III, 2025]. In this view, there is no physical matter inside the event horizon contributing additional mass; the central object is an Aether-density structure anchored by the global galactic ledger. Neutron-star–initiated black holes appear only as transient seeds in which collapsed matter briefly

triggers the Aether-density configuration before evaporating. The extremal galactic-center condition $M/r = m_a/\lambda_C$ with curl = 1 drives the Aether fine structure to a value of order 10^{-48}, far below the electron-sector fine structure α, and marks a ledger point that cannot be approached by any laboratory system based on electron mass and ordinary materials.

The bipolar double-trumpet Tesla coil is proposed as a laboratory toy model that implements the torsion *phase structure* in a controllable way, in the spirit of analogue gravity experiments but focused on Aether torsion [Barceló et al., 2011, Steinhauer, 2016, Jacquet et al., 2020]. The horn ring and primary represent the black hole horizon and accretion ring; the conical secondaries represent the bipolar torsion channels; and the remote top loads represent distant anchor regions in the Aether. By measuring filamentary structures around the ring, axial channels along the cones, and phase-based path-shortening effects in the Aether geometry of the coil, one can test the torsion laws without creating a black hole, without concentrating physical matter inside an event horizon, and without violating the QMU photon-speed ledger. The toy model shares the same curl unit curl and the same dimensionless torsion invariants, but it lives entirely in the electron and laboratory-field sector, far from the galactic-center ledger scale.

This work suggests several directions for further research:

- Extend the derivation of Ξ_{mag} and Ξ_{elec} from the Aether Lagrangian to include explicit dependence on galactic-scale parameters, using the black-hole parameterization developed in Thomson III [2025].
- Refine the path-shortening analysis in the coil to include detailed chronovibrational phase measurements, using synchronized sources and detectors at the horn and top loads, and cross-checking with independent QMU chronovibrational ledgers [Thomson, 2025b].
- Apply the filament–jet reciprocity ledger to specific astrophysical systems, using observational data on filament networks, jet morphology, and potential gradients to constrain $(\Xi_{\text{mag}}, \Xi_{\text{elec}})$ in AGN, blazars, and microquasars [Blandford et al., 2019, Remillard and McClintock, 2006, Fender et al., 2004, Event Horizon Telescope Collaboration, 2019].
- Use the coil as a testbed for more complex Aether torsion configurations, such as multiple jets, misaligned disks, or time-varying torsion phases, and compare with state transitions in X-ray binaries [Remillard and McClintock, 2006, Fender et al., 2004].

The combination of black hole torsion physics and double-trumpet coil experiments in QMU provides a path toward a unified understanding of torsion filaments, polar jets, and path-shortened Aether channels in both astrophysical and laboratory settings, while keeping the scale separation between galactic-center Aether fine structure and electron-sector laboratory systems explicitly in view.

Acknowledgments

The author thanks the Quantum AetherDynamics Institute community and computational collaborators for continued work on Aether torsion, trumpet coil experiments, and the development of Quantum Measurement Units.

References

Carlos Barceló, Stefano Liberati, and Matt Visser. Analogue gravity. *Living Rev. Relativ.*, 14(3), 2011. doi: 10.12942/lrr-2011-3.

R. D. Blandford and D. G. Payne. Hydromagnetic flows from accretion discs and the production of radio jets. *Mon. Not. R. Astron. Soc.*, 199(4):883–903, 1982. doi: 10.1093/mnras/199.4.883.

R. D. Blandford and R. L. Znajek. Electromagnetic extraction of energy from kerr black holes. *Mon. Not. R. Astron. Soc.*, 179(3):433–456, 1977. doi: 10.1093/mnras/179.3.433.

Roger Blandford, David Meier, and Anthony Readhead. Relativistic jets from active galactic nuclei. *Annu. Rev. Astron. Astrophys.*, 57:467–509, 2019. doi: 10.1146/annurev-astro-081817-051948.

Event Horizon Telescope Collaboration. First M87 event horizon telescope results. i. the shadow of the supermassive black hole. *Astrophys. J. Lett.*, 875(1):L1, 2019. doi: 10.3847/2041-8213/ab0ec7.

R. P. Fender, T. M. Belloni, and E. Gallo. Towards a unified model for black hole x-ray binary jets. *Mon. Not. R. Astron. Soc.*, 355(4):1105–1118, 2004. doi: 10.1111/j.1365-2966.2004.08384.x.

Maxime J. Jacquet, Florian Koening, Renaud Parentani, Stefano Finazzi, and Silke Weinfurtner. The next generation of analogue gravity experiments. *Phil. Trans. R. Soc. A*, 378(2177):20190239, 2020. doi: 10.1098/rsta.2019.0239.

João F. S. Melo and Fernando A. S. Neves. Improvements to secondary windings of tesla transformers using non-uniform pitch helical resonators. *Appl. Phys. Res.*, 13(2):23–33, 2021. doi: 10.5539/apr.v13n2p23.

I. F. Mirabel and L. F. Rodríguez. Sources of relativistic jets in the galaxy. *Annu. Rev. Astron. Astrophys.*, 37:409–443, 1999. doi: 10.1146/annurev.astro.37.1.409.

Mark Morris and Eric Serabyn. The galactic center environment. *Annu. Rev. Astron. Astrophys.*, 34:645–701, 1996. doi: 10.1146/annurev.astro.34.1.645.

M. O. Reed, M. T. Hummon, S.-W. Nam, and R. P. Mirin. A conduction-coupled tesla transformer. *Rev. Sci. Instrum.*, 86(3):035113, 2015. doi: 10.1063/1.4913672.

M. J. Rees. Appearance of relativistically expanding radio sources. *Nature*, 211(5052):468–470, 1966. doi: 10.1038/211468a0.

Ronald A. Remillard and Jeffrey E. McClintock. X-ray properties of black-hole binaries. *Annu. Rev. Astron. Astrophys.*, 44:49–92, 2006. doi: 10.1146/annurev.astro.44.051905.092532.

Jeff Steinhauer. Observation of quantum hawking radiation and its entanglement in an analogue black hole. *Nature Phys.*, 12(10):959–965, 2016. doi: 10.1038/nphys3863.

Nikola Tesla. *Experiments with Alternate Currents of High Potential and High Frequency*. McGraw Publishing, New York, 1893. Classic lectures on resonant transformers and coil geometries.

David W. Thomson and Jim Bourassa. *Secrets of the Aether*. Aenor Trust, Portland, OR, 2004. doi: 10.13140/2.1.1633.7926. Foundational exposition of the Aether Physics Model (APM).

David W. III Thomson. Torsion filament law applied to intergalactic filaments: Predicting substructures and helicity in the cosmic web. *Zenodo*, 2025a. doi: 10.5281/zenodo.17888143. Quantum AetherDynamics Institute (QADI) preprint.

David W. III Thomson. Mass–energy ledgers in QMU and relativity: Constructive aether geometry versus principle theory. *Zenodo*, 2025b. doi: 10.5281/zenodo.17849475. Quantum AetherDynamics Institute (QADI) preprint.

David W. III Thomson. Superconducting electron pair ledger in QMU: Aether dipoles, chronovibration, and magnetic cancellation. *Zenodo*, 2025c. doi: 10.5281/zenodo.17886298. Quantum AetherDynamics Institute (QADI) preprint.

David W. III Thomson. Torsion filament law in QMU: Predicting number, spacing, and angles around supermassive objects. *Zenodo*, 2025d. doi: 10.5281/zenodo.17873880. Quantum AetherDynamics Institute (QADI) preprint.

David W. Thomson III. Aether lagrangian for galactic black hole parameters. *Physics Essays*, 38(1): 1–9, 2025. doi: 10.4006/0836-1398-38.1.1. URL https://doi.org/10.4006/0836-1398-38.1.1.

C. Megan Urry and Paolo Padovani. Unified schemes for radio-loud active galactic nuclei. *Publ. Astron. Soc. Pac.*, 107(715):803–845, 1995. doi: 10.1086/133630.

F. Yusef-Zadeh, M. Morris, and D. Chance. Large-scale nonthermal radio filaments in the galactic center. *Nature*, 310(5980):557–561, 1984. doi: 10.1038/310557a0.

Farhad Yusef-Zadeh. The origin of the galactic center nonthermal radio filaments: Young stellar clusters? *Astrophys. J.*, 598(1):325–339, 2003. doi: 10.1086/378866.